SIMULTANEOUS OPTIMIZATION OF MATERIAL REMOVAL RATE AND SURFACE ROUGHNESS IN ULTRASONIC VIBRATION-ASSISTED EDM OF HARDOX 500 USING NSGA-II AND MABAC

TỐI ƯU HÓA ĐỒNG THỜI NĂNG SUẤT BÓC TÁCH VẬT LIỆU VÀ ĐỘ NHÁM BỀ MẶT TRONG GIA CÔNG TIA LỬA ĐIỆN CÓ HỖ TRỢ RUNG ĐỘNG SIÊU ÂM TRÊN THÉP HARDOX 500 BẰNG PHƯƠNG PHÁP NSGA-II VÀ MABAC

Tran Huu Danh[1], Nguyen Cong Danh[2], Mai Tat Loi [3], Vu Ngoc Pi[4], Nguyen Manh Cuong[4,*]

[1]Vinh Long University of Technology Education (Long Chau ward, Vinh Long province)

[2]Vinh Long Vocational College (Phu Quoi commune, Vinh Long province)

[3]Vinh University of Technology Education (Truong Vinh ward, Nghe An province)

[4]Thai Nguyen University of Technology, Thai Nguyen University

**Email: nmcuong@tnut.edu.vn*

ABSTRACT

In this study, a multi-objective optimization framework is proposed for ultrasonic vibration-assisted electrical discharge machining (UV-EDM) of HARDOX 500 steel. The main objectives are to simultaneously maximize the material removal rate (MRR) and minimize the surface roughness (Ra), which represent productivity and surface quality, respectively. Experimental data were modeled using Gaussian process regression (GPR), and the optimization problem was solved with the Non-dominated Sorting Genetic Algorithm II (NSGA-II) to generate a Pareto front of trade-off solutions. To support decision-making, the Multi-Attributive Border Approximation area Comparison (MABAC) method was applied to select the most balanced solution from the Pareto set. The results demonstrate that the proposed NSGA-II–MABAC hybrid approach effectively identifies optimal machining parameters, providing a favorable compromise between high MRR and low Ra. The evolution of Pareto fronts across generations confirmed the convergence behavior of NSGA-II, while the knee-point analysis further validated the trade-off characteristics. This integrated framework offers a robust methodology for achieving simultaneous productivity and surface integrity in ultrasonic-assisted EDM of hard-to-machine materials such as HARDOX 500, and it can be extended to other advanced machining processes.

Keywords: *Ultrasonic vibration-assisted EDM; HARDOX 500 steel; Multi-objective optimization; Material removal rate (MRR); Surface roughness (Ra); NSGA-II; MABAC.*

TÓM TẮT

Nghiên cứu này đề xuất một khung tối ưu hóa đa mục tiêu cho quá trình gia công tia lửa điện vật liệu thép HARDOX 500 có hỗ trợ rung động siêu âm (UV-EDM). Các mục tiêu chính là đồng thời tối đa hóa năng suất bóc tách vật liệu (MRR) và tối thiểu hóa độ nhám bề mặt (Ra), đại diện *lần lượt cho năng suất và chất lượng bề mặt. Dữ liệu thực nghiệm được mô hình hóa bằng Gaussian Process Regression (GPR), và bài toán tối ưu được giải bằng giải thuật di truyền phân loại không trội NSGA-II để xây dựng biên Pareto các nghiệm đánh đổi. Để hỗ trợ ra quyết định, phương pháp MABAC (Multi-Attributive Border Approximation area Comparison) được áp dụng nhằm chọn ra nghiệm cân bằng nhất từ tập Pareto. Kết quả cho thấy cách tiếp cận lai NSGA-II–MABAC đề xuất đã xác định hiệu quả các thông số gia công tối ưu, mang lại sự thỏa hiệp hợp lý giữa MRR cao và Ra thấp. Quá trình tiến hóa các biên Pareto qua các thế hệ khẳng định khả năng hội tụ của NSGA-II, đồng thời phân tích điểm gối (knee-point) xác nhận rõ ràng đặc trưng đánh đổi. Khung tích hợp này cung cấp một phương pháp tiếp cận mạnh mẽ để đạt đồng thời năng suất và chất lượng bề mặt trong EDM có hỗ trợ siêu âm trên vật liệu khó gia công như HARDOX 500, và có thể mở rộng cho các quá trình gia công tiên tiến khác.*

Từ khóa: *Gia công tia lửa điện có hỗ trợ rung động siêu âm; Thép HARDOX 500; Tối ưu hóa đa mục tiêu; Năng suất bóc tách vật liệu (MRR); Độ nhám bề mặt (Ra); NSGA-II; MABAC.*

1. INTRODUCTION

Electrical discharge machining (EDM) has been widely applied for machining difficult-to-cut materials, yet its performance is often constrained by issues of low material removal rate (MRR), poor surface integrity, and inefficient debris evacuation. To overcome these limitations, UV-EDM has been extensively explored, as the introduction of ultrasonic vibration can enhance debris removal, improve flushing efficiency, and stabilize the discharge process. For instance, Wang et al. [1] demonstrated that the use of longitudinal and torsional ultrasonic vibrations in deep-hole EDM effectively suppressed taper formation and enhanced debris motion. Similarly, Zhang et al. [2] clarified the mechanisms of debris removal during ultrasonic EDM drilling, showing improved machining stability compared to conventional EDM. Yin et al. [3] proposed a novel EDM method using longitudinal-torsional vibration electrodes for micro-holes, reporting substantial improvements in machining quality and efficiency.

At the micro-scale, Chenxue et al. [4] investigated bubble behavior under ultrasonic vibration in EDM, confirming the role of cavitation in stabilizing discharges. Li et al. [5] explored two-dimensional ultrasonic circular vibration (UCV) electrodes for micro-EDM and revealed better surface integrity, while Li et al. [6] earlier established that UCV electrodes can significantly improve micro-hole machining performances. Lei et al. [7] extended the concept by applying laminated electrodes in UV-EDM of enclosed microgrooves, which improved dimensional accuracy and machining throughput. These works emphasize that ultrasonic vibration, whether applied to the tool, workpiece, or electrode, fundamentally alters discharge conditions and enhances machining outcomes.

Beyond machining mechanisms, hybrid processes have been explored. Han et al. [8] investigated ultrasonic vibration-assisted powder-mixed EDM of TiN ceramics and reported improved surface finish with enhanced MRR. Lin et al. [9] earlier demonstrated that combining EDM with ultrasonic vibration and abrasive jet machining could improve machining efficiency, while Prihandana et al. [10] analyzed micro-powder suspension and ultrasonic vibration in dielectric fluid, validating ☞

Taguchi-based optimization to enhance micro-EDM performance. More recently, Dong et al. [11] employed thermodynamic simulations and experiments to evaluate vertical UV-EDM, confirming its potential for machining hard alloys. These studies highlight diverse configurations of UV-EDM and the continuous trend toward hybridized processes.

Theoretical and numerical modeling has also contributed to understanding process mechanisms. Singh et al. [12] presented finite element modeling of ultrasonic vibration-assisted EDM, providing insights into discharge energy distribution, while Shervani-Tabar et al. [13] investigated simultaneous ultrasonic vibration of tool and workpiece, showing synergetic effects on machining stability. Such studies provide a foundation for predictive modeling and optimization in UV-EDM.

Despite these advances, challenges remain in systematically optimizing multiple conflicting performance measures, particularly in machining advanced materials such as HARDOX 500 steel, known for its high hardness and wear resistance. While prior works [1-6, 10-13] demonstrate improvements in either productivity or surface quality, few studies have considered simultaneous optimization of MRR and Ra under UV-EDM conditions. Moreover, while multi-objective evolutionary algorithms like NSGA-II have been applied in EDM contexts, limited research has combined them with multi-criteria decision-making (MCDM) methods such as MABAC to identify the most balanced solution from the Pareto front. This creates a research gap in developing a hybrid optimization and decision-support framework tailored for UV-EDM of HARDOX 500.

Therefore, the objective of this study is to address this gap by integrating GPR-based modeling with NSGA-II for multi-objective optimization, and applying the MABAC method for decision support. Specifically, the goals are to simultaneously maximize MRR and minimize Ra in UV-EDM of HARDOX 500 steel. By combining evolutionary optimization with decision-making analysis, this work contributes a robust methodology for enhancing both productivity and surface quality in machining ultra-hard steels, while providing a systematic framework extendable to other advanced EDM processes.

2. METHODOLOGY

2.1. NSGA-II for Multi-Objective Optimization

The NSGA-II is one of the most widely applied evolutionary algorithms for solving multi-objective optimization problems due to its elitist mechanism, fast non-dominated sorting, and crowding distance-based diversity preservation. In this study, NSGA-II is employed to optimize two conflicting objectives in UV-EDM of HARDOX 500 steel: maximizing the MRR and minimizing the Ra.

The algorithm begins with the initialization of a population of candidate solutions generated within the ranges of machining parameters (pulse on-time, pulse off-time, discharge current, gap voltage, and vibration amplitude). Each individual solution is evaluated using GPR surrogate models that predict MRR and Ra from the process parameters.

The main steps of NSGA-II are as follows:

1) Fast Non-dominated Sorting: The population is ranked into multiple Pareto fronts based on non-dominance relationships.

2) Crowding Distance Assignment: To maintain diversity, the crowding distance of each individual in a front is computed.
3) Selection: A binary tournament selection based on Pareto rank and crowding distance is used to select parents.
4) Crossover and Mutation: Offspring solutions are generated through simulated crossover and Gaussian mutation.
5) Elitism: Parents and offspring are merged, and the best individuals are selected to form the next generation.

Through iterative evolution, NSGA-II converges to a Pareto-optimal front that represents the trade-off set of machining solutions balancing Ra and MRR.

2.2. MABAC for Multi-Criteria Decision Making

The MABAC method, introduced by Pamucar and Cirovic in 2015, is employed to rank the Pareto-optimal solutions obtained by NSGA-II. Unlike classical multi-criteria decision-making (MCDM) methods, MABAC ranks alternatives based on their relative distances to a defined "border approximation area", thereby allowing a robust and interpretable decision process.

The MABAC procedure consists of the following steps [14]:

*Step 1: Build the initial decision-making matrix

$$X = \begin{bmatrix} r_{11} & \cdots & r_{1j} & \cdots & r_{1n} \\ \vdots & \ddots & \vdots & \ddots & \vdots \\ r_{1} & \cdots & r_{ij} & \cdots & r_{in} \\ \vdots & \ddots & \vdots & \ddots & \vdots \\ r_{m1} & \cdots & r_{mj} & \cdots & r_{mn} \end{bmatrix}_{m \times n} \quad (1)$$

Where: m is the number of alternatives and n is the number of criteria.

*Step 2: Normalize the decision matrix

For each criterion, the normalized values are calculated as:

$$r_{ij}^{*} = \frac{r_{ij} - r_i^{-}}{r_i^{+} - r_i^{-}} \quad (2)$$

$$r_{ij}^{*} = \frac{r_{ij} - r_i^{+}}{r_i^{-} - r_i^{+}} \quad (3)$$

In which, i = 1,2, ...,m and j = 1,2, ...,n. Equation (2) is applied for criteria MRR, and (3) is applied for Ra. Also, $r_i^{+} = \max(r_1, r_2, \ldots, r_m)$ and $r_i^{-} = \min(r_1, r_2, \ldots, r_m)$.

*Step 3: Compute the weighted normalized matrix

$$v_{ij} = w_j + w_j \times r_{ij}^{*} \quad (4)$$

*Step 4: Calculate the border approximation area for each criterion

$$g_j = \left(\prod_{i=1}^{m} v_{ij}\right)^{1/m} \quad (5)$$

*Step 5: Determine the distance of each alternative from the border approximation area

$$q_{ij} = v_{ij} - g_i \quad (6)$$

Where: i = 1,2, ...,m and j = 1,2, ...,n.

*Step 6: Calculate the total distance for each alternative

$$S_i = \sum_{j=1}^{n} q_{ij} \quad i = 1, 2, \ldots, m \quad (7)$$

*Step 7: Rank the alternatives by maximizing S.

☞

3. EXPERIMENTAL WORK

Figure 1 illustrates the experimental setup employed in this study. All machining experiments were performed on a Sodick A30 CNC EDM system, which was modified to integrate a high-power ultrasonic vibration module. The integration of ultrasonic vibration aimed to enhance spark stability, improve dielectric flushing efficiency, and promote more effective debris evacuation during the machining of hard materials such as HARDOX 500 steel.

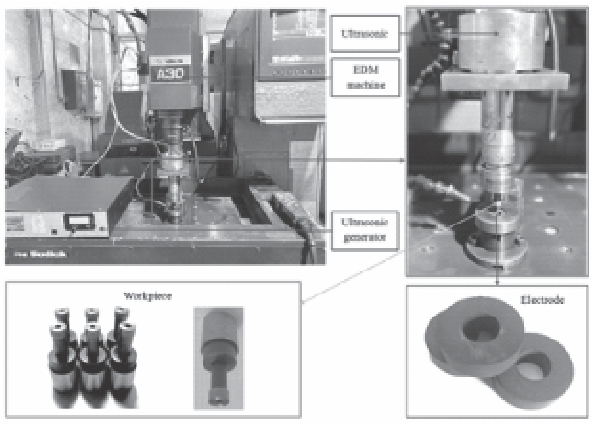

Figure 1. Experimental setup

Ultrasonic vibrations were generated using an MPI WG-3000 ultrasonic generator (MPI Ultrasonics, Switzerland) with a rated power of 3000 W. These vibrations were transmitted through an RPS-5020-4Z ultrasonic transducer operating at a frequency of 20 kHz and a nominal power of 2000 W. To efficiently transfer vibratory energy into the machining zone, a custom-fabricated titanium horn was employed. The horn provided consistent vibratory motion at the tool–workpiece interface, which is critical for maintaining uniform spark distribution and enhancing the dielectric flushing mechanism.

The tool electrode used was HK2 graphite, selected due to its excellent electrical conductivity and favorable wear resistance in EDM applications. The dielectric fluid was Diel MS 7000 (Total, France), a commercial EDM oil chosen for its stable discharge characteristics and high thermal resistance. The workpiece material was HARDOX 500 steel, a quenched and tempered alloy known for its high hardness and abrasion resistance. Cylindrical specimens were prepared to facilitate uniform flushing conditions and consistent surface roughness evaluation.

Two performance indicators were considered as the output responses: MRR and Ra. The MRR was determined using the gravimetric method, which offers high precision and reproducibility in EDM research. Prior to machining, each specimen was cleaned with ethanol, dried with warm air, and weighed using an analytical balance with a resolution of 0.1 mg. Following machining, the same cleaning and drying procedure was repeated before reweighing. The MRR (g/h) was calculated as:

$$MRR = \frac{m_{before} - m_{after}}{t} \cdot 3600 \quad (8)$$

Where: m_{before} and m_{after} represent the masses of the workpiece before and after machining (g), and t is the machining time (s).

The Ra of the machined surfaces was measured using a Mitutoyo SV3100 surface roughness tester. To ensure reliability and representativeness, three measurements were taken at different positions along the external cylindrical surface of each specimen, and their average was reported as the final Ra.

The experimental design was based on the Box–Behnken Design (BBD), which is particularly suitable for response surface modeling involving multiple variables while minimizing the number of required experimental runs. Five input parameters were selected for investigation: A, T_{on}, T_{off}, IP, and SV. Each parameter was studied at three levels (low, medium, high), with ranges determined through preliminary trials and bounded by the operational limits of the EDM system and ultrasonic module.

The complete experimental matrix, along with the measured responses of MRR and Ra for each run, is presented in Table 1.

4. RESULTS AND DISCUSSION

4.1. Performance of GPR Models

GPR models were developed to predict the machining responses Ra and MRR from the five input variables (A, T_{on}, T_{off}, IP, and SV). The predictive accuracy of the models was first evaluated using training and five-fold cross-validation datasets. For Ra, the GPR model achieved an R^2 of 0.95 on training and 0.59 on cross-validation, indicating that although the model fit the experimental data well, predictive accuracy under unseen data conditions was moderately limited. In contrast, the MRR model yielded R^2 values of 0.94 (training) and 0.86 (cross-validation), demonstrating robust predictive capability. The predicted versus actual plots (Figure 2) confirm that GPR provides reliable surrogates for subsequent optimization, particularly for MRR.

Table 1. Experimental matrix and measured responses (MRR and Ra)

No.	A (µm)	T_{on} (µs)	T_{off} (µs)	IP (A)	SV (V)	MRR (g/h)	Ra (µm)
1	1.2	8	12	10	5	3.346	3.353
2	1.2	16	12	10	5	1.482	6.569
3	5.2	8	12	10	5	3.119	3.198
4	5.2	16	12	10	5	1.228	5.711
5	3.2	12	8	5	5	1.210	7.220
6	3.2	12	8	15	5	3.665	6.764
7	3.2	12	16	5	5	1.317	6.462
8	3.2	12	16	15	5	4.013	7.260
9	3.2	8	12	10	4	3.293	3.175
10	3.2	8	12	10	6	3.211	3.201
11	3.2	16	12	10	4	1.572	5.889
12	3.2	16	12	10	6	1.416	6.588
13	1.2	12	8	10	5	3.474	5.418
14	1.2	12	16	10	5	3.850	4.492
15	5.2	12	8	10	5	4.073	5.444
16	5.2	12	16	10	5	3.832	4.959
17	3.2	12	12	5	4	1.347	6.339
18	3.2	12	12	5	6	1.274	5.968

19	3.2	12	12	15	4	3.732	6.726
20	3.2	12	12	15	6	4.167	7.312
21	3.2	8	8	10	5	4.216	3.430
22	3.2	8	16	10	5	3.290	3.256
23	3.2	16	8	10	5	1.391	7.280
24	3.2	16	16	10	5	1.360	5.313
25	1.2	12	12	5	5	1.351	6.730
26	1.2	12	12	15	5	3.943	7.595
27	5.2	12	12	5	5	1.243	6.099
28	5.2	12	12	15	5	3.993	8.799
29	3.2	12	8	10	4	4.010	5.790
30	3.2	12	8	10	6	4.069	5.019
31	3.2	12	16	10	4	4.046	5.287
32	3.2	12	16	10	6	4.041	5.479
33	1.2	12	12	10	4	3.759	4.408
34	1.2	12	12	10	6	3.746	5.259
35	5.2	12	12	10	4	3.853	6.312
36	5.2	12	12	10	6	3.811	5.564
37	3.2	8	12	5	5	1.444	2.965
38	3.2	8	12	15	5	3.364	3.850
39	3.2	16	12	5	5	0.969	7.694
40	3.2	16	12	15	5	1.566	12.089
41	3.2	12	12	10	5	3.733	4.483
42	3.2	12	12	10	5	3.829	4.919
43	3.2	12	12	10	5	3.822	5.483
44	3.2	12	12	10	5	3.799	5.032
45	3.2	12	12	10	5	3.764	5.455
46	3.2	12	12	10	5	3.775	4.785

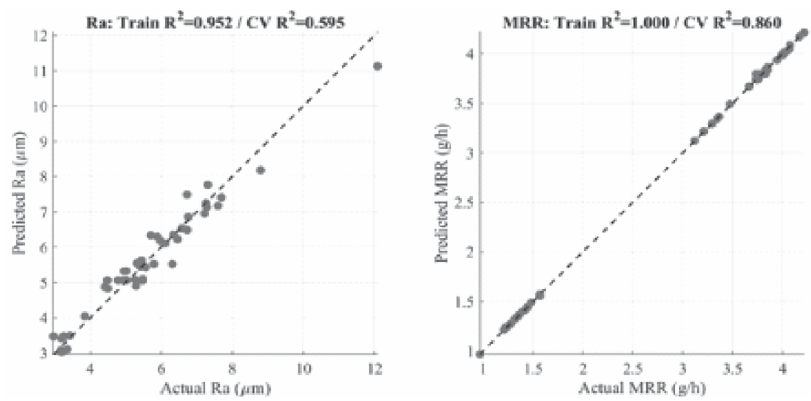

Figure 2. Predicted versus actual values of (a) Ra and (b) MRR using GPR models

4.2. Pareto Front Generation Using NSGA-II

To provide a clear overview of all experimental results, Figure 2 illustrates the AHP Score for each experiment, with the best-performing configuration (Rank 1) highlighted in red.

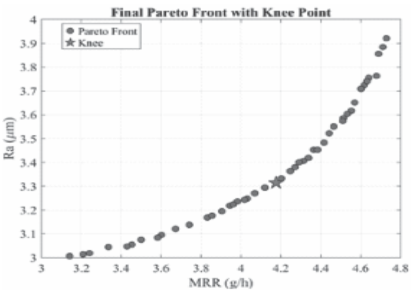

Figure 3. Final Pareto front with identification of the knee-point solution

The NSGA-II was applied to simultaneously minimize Ra and maximize MRR. Over 100 generations with a population size of 50, NSGA-II demonstrated consistent convergence. The Pareto front obtained (Figure 3) reveals a distinct trade-off relationship: lower Ra values are achievable at the expense of reduced MRR, and vice versa. This trade-off reflects the inherent conflict between surface quality and productivity in EDM. The spread and density of solutions indicate that NSGA-II effectively preserved population diversity, thereby enabling a comprehensive exploration of the solution space.

4.3. Selection of Optimal Solution Using MABAC

While the Pareto front provides multiple non-dominated alternatives, decision-making support is required to identify the most balanced solution. The MABAC method was employed to rank Pareto solutions based on their relative distances from a defined border approximation area. Results showed that the optimal solution selected by MABAC corresponded to machining parameters of approximately A = 3.90 μm, T_{on} = 9.08 μs, T_{off} = 8.18 μs, IP = 11.63 A, and SV = 5.32 V, yielding Ra = 3.92 μm and MRR = 4.73 g/h. This solution prioritizes higher productivity with a moderate compromise in surface quality compared to the knee-point solution.

4.4. Knee-Point Analysis

In addition to MABAC, the knee-point of the Pareto front was identified using the chord distance method (Figure 3). The knee-point represents the most balanced compromise between the two objectives. The selected knee solution achieved Ra ≈ 3.31 μm and MRR ≈ 4.19 g/h. Compared with the MABAC solution, the knee-point emphasized improved surface quality at the cost of slightly lower material removal rate. This confirms the complementary roles of MABAC and knee-point analysis: while MABAC selects the best-ranked alternative based on a global decision matrix, the knee-point provides a purely geometric criterion for balance.

4.5. Discussion

The results confirm that the integration of NSGA-II with MABAC provides a systematic and effective decision-support framework for UV-EDM optimization. The Pareto front clearly illustrates the conflict between Ra and MRR in machining HARDOX 500, while the use of GPR ensures efficient and accurate evaluation of candidate solutions. The MABAC solution highlights productivity-oriented optimization, whereas the knee-point emphasizes balanced surface quality. Together, these approaches offer valuable flexibility to decision-makers, depending on whether production throughput or surface integrity is prioritized. Importantly, the proposed framework can be generalized to other hard-to-machine materials and hybrid EDM configurations, demonstrating its broader applicability in advanced manufacturing optimization. ☞

5. CONCLUSION

In this study, a hybrid framework combining GPR, the NSGA-II, and the MABAC method was developed and applied to the UV-EDM of HARDOX 500 steel. The following conclusions can be drawn:

1) GPR models provided accurate predictive capability for both Ra and MRR, with the MRR model showing particularly strong generalization performance, thereby enabling efficient surrogate-assisted optimization.

2) NSGA-II successfully generated a well-distributed Pareto front, highlighting the trade-off relationship between minimizing surface roughness and maximizing material removal rate. Convergence analysis using the hypervolume indicator confirmed the robustness of the optimization process.

3) The MABAC method effectively ranked Pareto solutions and identified an optimal set of parameters (A ≈ 3.90 µm, T_{on} ≈ 9.08 µs, T_{off} ≈ 8.18 µs, IP ≈ 11.63 A, SV ≈ 5.32 V), yielding Ra ≈ 3.92 µm and MRR ≈ 4.73 g/h. This solution emphasizes higher productivity with a moderate compromise in surface quality.

4) Knee-point analysis provided an alternative compromise solution (Ra ≈ 3.31 µm, MRR ≈ 4.19 g/h), which favors surface quality at the expense of slightly reduced productivity. The complementarity of MABAC ranking and knee-point selection highlights the flexibility of the proposed framework in decision support.

Acknowledgments:

This work was supported by Ministry of Education and Training of Vietnam (MOET) through Project B2024-TNA-18.❖

References:

[1]. P. Wang et al., "*Debris motion and taper suppression in EDM deep hole machining assisted by longitudinal/torsional ultrasonic vibration*". Journal of Manufacturing Processes, vol. 133, pp. 798-810, 2025.

[2]. P. Zhang et al., "*Investigating mechanisms of debris removal in ultrasonic vibration-assisted EDM drilling*". International Journal of Mechanical Sciences, vol. 279, p. 109486, 2024.

[3]. Z. Yin et al., "*A novel EDM method using longitudinal-torsional ultrasonic vibration (LTV) electrodes to improve machining performance for micro-holes*". Journal of Manufacturing Processes, vol. 102, pp. 231-243, 2023.

[4]. W. CHENXUE, T. SASAKI, and A. HIRAO, "*Observation of bubble behavior in EDM with ultrasonic vibration*". Procedia CIRP, vol. 113, pp. 267-272, 2022.

[5]. Z. Li, J. Tang, Y. Li, and J. Bai, "*Investigation on surface integrity in novel micro-EDM with two-dimensional ultrasonic circular vibration (UCV) electrode*". J. Manuf. Process 76: 828-840," ed, 2022.

[6]. Z. Li, J. Tang, and J. Bai, "*A novel micro-EDM method to improve microhole machining performances using ultrasonic circular vibration (UCV) electrode*". International Journal of Mechanical Sciences, vol. 175, p. 105574, 2020.

[7]. J. Lei, H. Shen, H. Wu, W. Pan, X. Wu, and C. Zhao, "*Ultrasonic vibration-assisted electrical discharge machining of enclosed microgrooves with laminated electrodes*". Journal of Materials Research and Technology, vol. 30, pp. 9521-9530, 2024.

[8]. J. Han, X. Gao, Y. Zhou, Z. Li, M. Gao, and Q. Zhang, "*Machining characteristics in ultrasonic vibration-assisted powder-mixed electrical discharge machining of TiN ceramics*". Ceramics International, vol. 50, no. 8, pp. 13478-13489, 2024.

[9]. M. Xu, J. Zhang, Y. Li, Q. Zhang, and S. Ren, "*Material removal mechanisms of cemented carbides machined by ultrasonic vibration assisted EDM in gas medium*". Journal of Materials Processing Technology, vol. 209, no. 4, pp. 1742-1746, 2009.

[10]. G. S. Prihandana, M. Mahardika, M. Hamdi, Y. S. Wong, and K. Mitsui, "*Effect of micro-powder suspension and ultrasonic vibration of dielectric fluid in micro-EDM processes—Taguchi approach*". International Journal of Machine Tools and Manufacture, vol. 49, no. 12-13, pp. 1035-1041, 2009.

[11]. Y. Dong, J. Liu, G. Li, and Y. Wang, "*Thermodynamic simulation modeling analysis and experimental research of vertical ultrasonic vibration assisted EDM*". The International Journal of Advanced Manufacturing Technology, vol. 119, no. 7, pp. 5303-5314, 2022.

[12]. J. Singh, R. Walia, P. Satsangi, and V. Singh, "*FEM modeling of ultrasonic vibration assisted work-piece in EDM process*". International Journal of Mechanic Systems Engineering, vol. 1, no. 1, pp. 8-16, 2011.

[13]. M. T. Shervani-Tabar, K. Maghsoudi, and M. R. Shabgard, "*Effects of simultaneous ultrasonic vibration of the tool and the workpiece in ultrasonic assisted EDM*". International Journal for Computational Methods in Engineering Science and Mechanics, vol. 14, no. 1, pp. 1-9, 2013.